Articles

Physical Society of Indonesia

Journal of the Physical Society of Indonesia **2(1)**, 25-33 (2026)

https://doi.org/10.35895/jpsi.2.1.25-33.2026

Multiscale Atmospheric Drivers of the April 2023 Cilacap Flood: Insights from Himawari-9 RGB Imagery and Radiosonde Data

Jamrud Aminuddin[1*], Sri Susanti[1], Adnan Dendy Mardika[2], and Arief Darmawan[3]

[1]*Physics Study Program, Faculty of Mathematics and Natural Sciences, Jenderal Soedirman University, Central Java, 53122, Indonesia*
[2]*Meteorology, Climatology, and Geophysics Agency, Central Java, 50145, Indonesia*
[3]*Research Center for Climate and Atmosphere, National Research and Innovation Agency, Jakarta, 10340, Indonesia*

(Received October 11, 2026; revised January 17, 2026; accepted January 30, 2026; published online April 18, 2026)

This study analyzes the atmospheric drivers of extreme rainfall during the 27 April 2023 flood event in Cilacap, Indonesia, using satellite, reanalysis, and in situ data. Convective evolution was examined using rainfall records, Himawari-9 cloud-top temperatures, instability indices (CAPE, CIN, KI, TTI), and surface wind fields. Rainfall exceeded 135 mm from the afternoon to nighttime. Satellite observations showed rapid convective growth, with cloud-top temperatures dropping below −75 °C, indicating mature Cumulonimbus clouds. The 24-Hour Night Microphysics RGB imagery revealed convective initiation around 08:00 UTC and intensification during the evening. Atmospheric instability increased prior to the event, with CAPE exceeding 1600 J kg^{-1} between 09:00 and 12:00 UTC, while CIN decreased below 80 J kg^{-1}. Surface wind analysis identified a strong low-level convergence zone formed by moist onshore flow from the Indian Ocean interacting with inland winds. This convergence provided dynamical lifting that released the stored instability, triggering deep convection that peaked around 15:00 UTC. The results show that the extreme rainfall was driven by the coupling of high thermodynamic instability and local moisture convergence, demonstrating the value of combining NWP products and satellite RGB imagery for diagnosing coastal extreme rainfall.

Keywords: *Atmosphere, Clouds, Extreme, Himawari, Instability, Precipitation*

1. INTRODUCTION

Indonesia's position as a maritime continent with high solar radiation drives significant evaporation, resulting in high atmospheric moisture content. These conditions create an environment highly conducive to the formation of deep convective clouds, specifically Cumulonimbus (Cb). On 27 April 2023, the Cilacap region experienced an extreme precipitation event exceeding 150 mm, which triggered catastrophic flooding and surpassed the intensity of the historical 1992 flood. Cilacap's unique coastal geography, situated between the Indian Ocean and the southern Java mountain range, facilitates complex multiscale atmospheric interactions where regional phenomena, such as the Madden-Julian Oscillation (MJO) and the West Monsoon, enhance moisture transport toward the mainland.

Despite the high hydrometeorological risks in this area, a prominent research gap exists, as previous local studies have primarily utilized isolated approaches, relying either exclusively on Numerical Weather Prediction (NWP) methods or satellite-based RGB visualization. There is a lack of integrated research that combines these methodologies to analyze the gradual evolution of convective systems in the southern coastal region of Java. Consequently, a more comprehensive diagnosis is required to quantify the relationship between physical atmospheric parameters and the distinct developmental phases of clouds responsible for extreme rainfall.

This study addresses this gap by integrating high-resolution Himawari-9 satellite imagery (10-minute temporal and 2-km spatial resolution) with atmospheric instability indices and radiosonde observations from the BMKG Cilacap station (ID: 96805). The novelty of this research lies in the

*Contact Author: jamrud.aminuddin@unsoed.ac.id

synergistic use of the 24-Hour Night Microphysics RGB technique and the quantification of instability parameters such as CAPE, CIN, and KI to track the Cb cloud life cycle from initiation to maturity. By analyzing surface wind patterns and coastal convergence, this study aims to provide a deep understanding of the vertical lifting mechanisms that triggered the extreme flooding in Cilacap.

2. METHOD

2.1 Data

This research employs a multi-source approach, integrating in-situ observational data, satellite remote sensing, and atmospheric reanalysis datasets to diagnose the triggering mechanisms of the extreme flood in Cilacap on April 27, 2023. Precipitation data were obtained from the *Global Satellite Mapping of Precipitation* (GSMaP) Gauge-near-real-time (GNRT) type in .csv format. This dataset provides hourly rainfall estimates corrected with ground-based rain gauge data to ensure quantitative accuracy during the observation period from 12:00 to 16:30 UTC.

The microphysical characteristics and life cycle of convective clouds were analyzed using Himawari-9 Level 2 satellite imagery, specifically the *Infrared (IR) Enhanced* and *24-Hour Night Microphysics* RGB products. These satellite data feature a high temporal resolution of 10 minutes and a spatial resolution of 2 km, enabling precise monitoring of cloud phase transitions. Furthermore, vertical atmospheric profiles were evaluated using radiosonde data from the official BMKG Cilacap station (Station ID: 96743) located at 7.73° S and 109.01° E. The data were retrieved via the University of Wyoming portal for the observation cycles at 00:00 UTC and 12:00 UTC. To support the analysis of atmospheric fluid dynamics, the *European Centre for Medium-Range Weather Forecasts* (ECMWF) ERA5 reanalysis dataset was utilized to extract wind vectors (u, v) and instability indices across various pressure levels.

2.2 Data Processing

Data processing was conducted systematically through the integration of several meteorological computing software packages, including Microsoft Excel, QGIS, SATAID, and GrADS. Satellite data visualization using SATAID focused on identifying Cloud Top Temperature (CTT) values and cloud morphological classification. In this study, a CTT threshold below -60°C was established as an indicator of deep convection. Cloud type identification during nighttime conditions was performed by applying the *24-Hour Night Microphysics* RGB composite technique, which combines brightness temperature differences between infrared channels to distinguish physical cloud characteristics. The color scheme interpretation used for this classification is presented in detail in Table 1.

Table 1 Interpretation RGB 24-Hour Night Microphysics

Color	Interpretation
	Thick clouds with high peaks (Cb)
	Thick clouds at medium altitudes
	Thick clouds at high levels
	Dust or sand
	Low clouds

Thermodynamic analysis was performed by calculating a series of atmospheric stability indices to quantify the potential for thunderstorm development. Key parameters calculated included *Convective Available Potential Energy* (CAPE), *Convective Inhibition* (CIN), *K-Index* (KI), *Lifted Index* (LI), and the *Total Totals Index* (TTI) based on standard meteorological formulations. To ensure data synchronization with global meteorological standards, all time variables are presented in Coordinated Universal Time (UTC). Finally, air mass lifting mechanisms were analyzed through surface wind convergence patterns at the 925 hPa level to map Low-Level Moisture Transport (LLMT) from the Indian Ocean, which served as the primary driver for the extreme rainfall in the region.

3. RESULTS AND DISCUSSION

3.1 Spatio-Temporal Rainfall Distribution

The first analysis was conducted on the spatial rainfall distribution to identify the areas most severely affected by the flood. Based on Figure 1, it is observed that the daily rainfall accumulation on April 27, 2023, was concentrated along the coastal regions of Cilacap. The highest rainfall values were detected in North Cilacap, reaching 177.8 mm, while South Cilacap ranged between 160.8 and 166.4 mm. This spatial pattern confirms that the convective cells triggering the flood had an extensive reach covering the entire urban area down to the coastline.

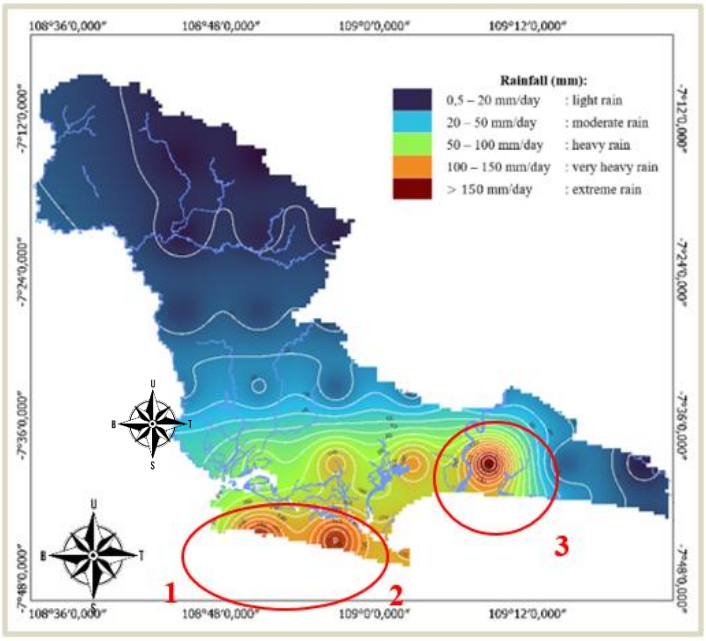

Figure 1 Spatial distribution of daily rainfall over Cilacap

Furthermore, to understand the timing of the extreme rainfall, a time-series analysis was performed, as presented in Figure 2. The graph indicates that the rainfall was not distributed evenly throughout the day but was concentrated during the night. A very sharp and simultaneous intensity spike is visible across the three primary observation points. Point 3 recorded the highest peak intensity, exceeding 135 mm at 15:00 UTC. The temporal synchronization of these peaks across all points suggests that the convective cloud system was a mature mesoscale system that developed uniformly over the Cilacap region, directly triggering an instantaneous rise in surface water discharge.

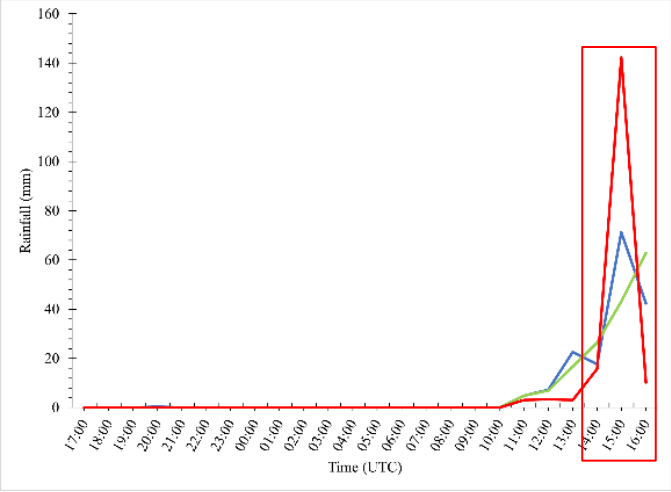

Figure 2 Time series of rainfall

3.2 Cloud Microphysics and Growth Characteristics

The analysis of the convective system's evolution was conducted by monitoring changes in the Cloud Top Temperature (CTT) across three observation points Figure 3. As shown in Figure 3(a) and Figure 3(b), a significant cooling trend is observed starting at 08:00 UTC, with temperatures progressively dropping below the -60°C threshold. Both locations maintained a mature deep convection phase from 10:00 to 16:00 UTC, indicating strong and persistent convective activity throughout the night.

However, Observation Point 3 Figure 3(c) displays a slightly different temporal pattern. Although convective initiation also began around 08:00 UTC, the mature phase was shorter, lasting only from 10:00 to 13:00 UTC. Despite these local variations, all three points reached their minimum temperature peaks of approximately -70°C at 15:00 UTC, confirming that a widespread mesoscale convective system covered the entire Cilacap region.

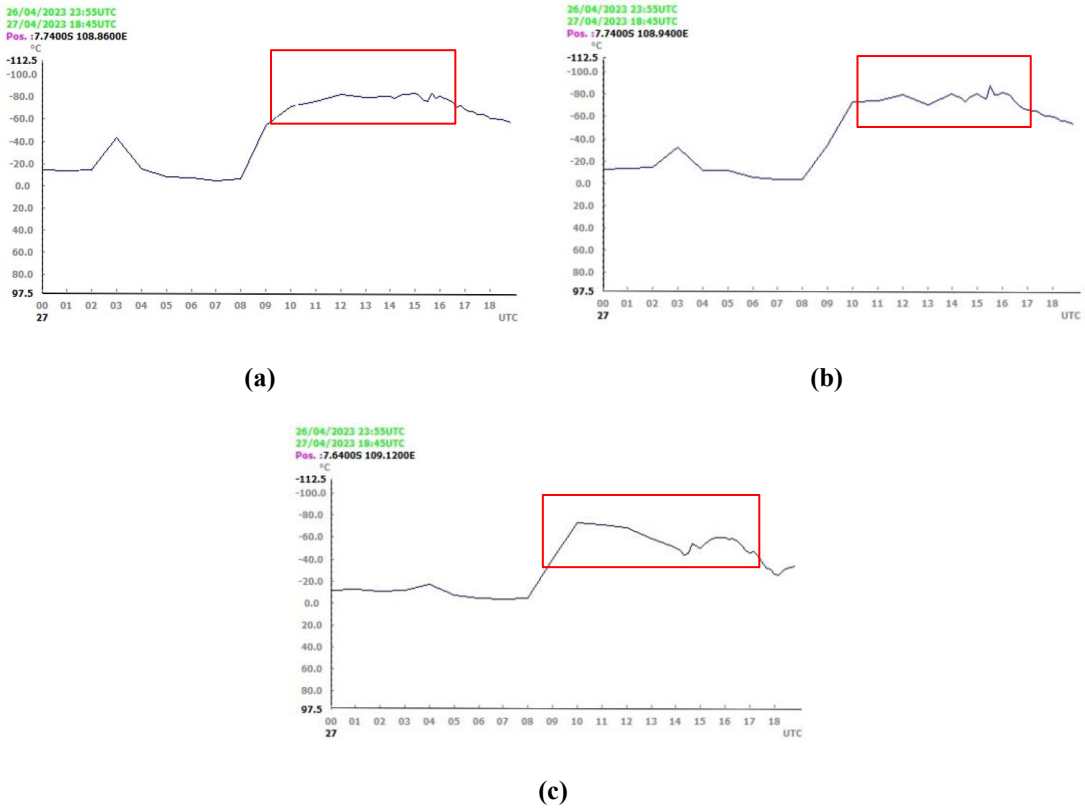

Figure 3 Time series of cloud surface temperature at (a) observation point 1, (b) observation point 2, and (c) observation point 3

The physical characteristics of these clouds were further confirmed through the 24-Hour Night Microphysics RGB satellite imagery in Figure 4. At 15:00 UTC, the Cilacap region was covered by a dense, dark brown-to-purple hue. Microphysically, this color scheme interprets the presence of very thick Cumulonimbus (Cb) clouds with high-altitude peaks containing large ice crystals. This specific color pattern distinguishes the Cb system from surrounding mid-level clouds, which appear yellowish.

The spatial distribution of the cloud top temperature over the observation area is presented as a contour visualization in Figure 5. This visualization shows that the convective cell core with the coldest temperatures (below $-60°C$) was centered directly over the Cilacap coast. The use of contours in this figure facilitates the identification of the mesoscale convective system's structure, which covers a vast area, aligning with the previously analyzed rainfall distribution.

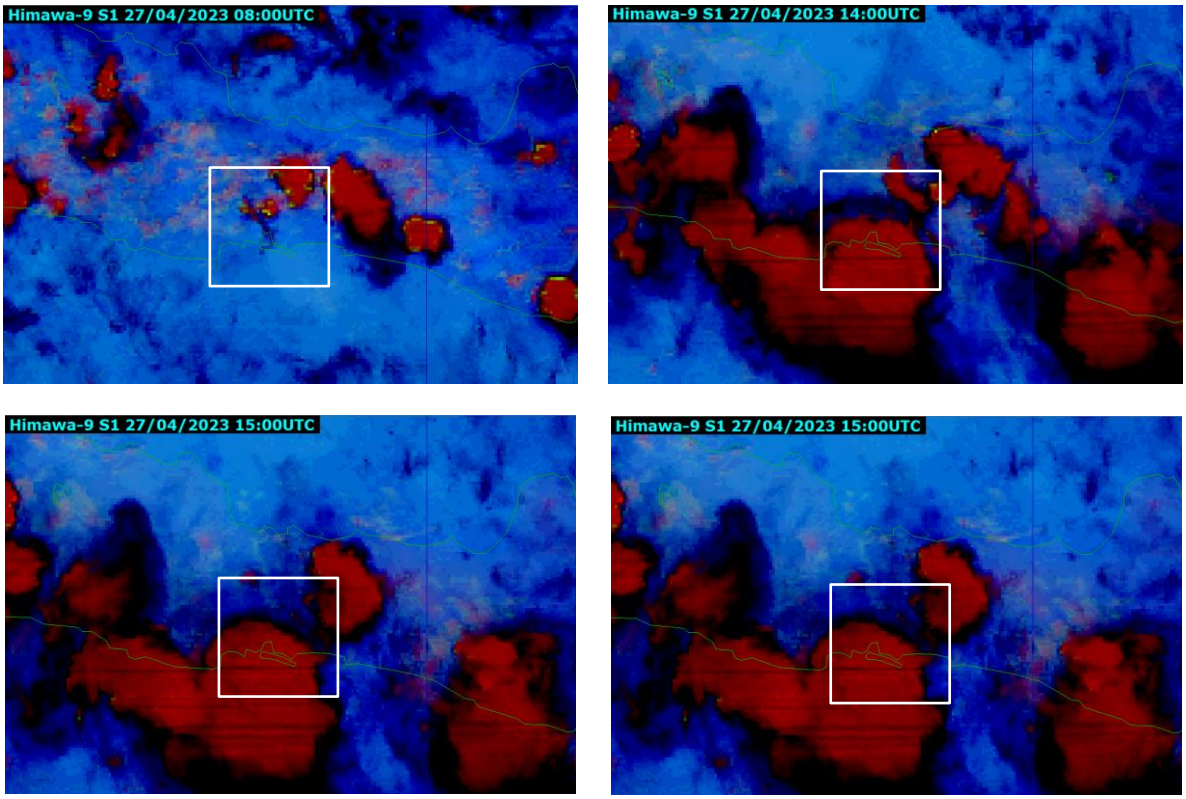

Figure 4 Satellite imagery with 24-hour Microphysics configuration on April 27, 2023.

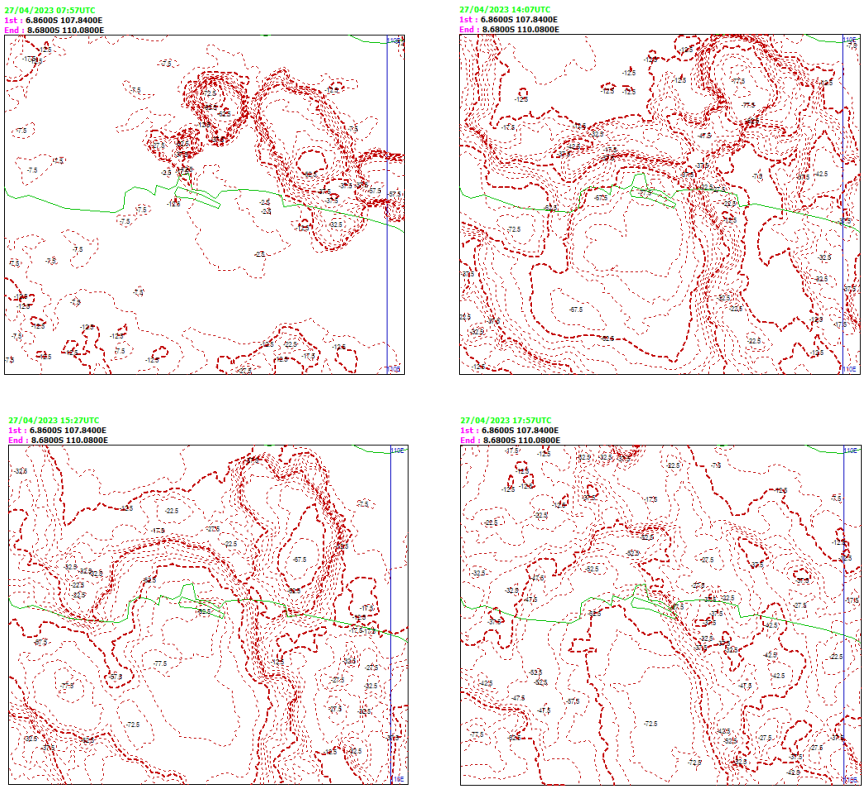

Figure 5 Cloud Contours on April 27, 2023

3.3 Atmospheric Instability Indices and Energy Release

The thermodynamic evolution of the atmosphere is analyzed through four key stability indices presented in Figure 6. The temporal variation of potential energy is illustrated in Figure 6(a), which shows a significant destabilization phase where Convective Available Potential Energy (CAPE) surged to a peak range of 1500–1600 J/kg between 09:00 and 12:00 UTC. This accumulation of potential energy coincided with conditions shown in Figure 6(b), where Convective Inhibition (CIN) values remained sufficiently low (below 80 J/kg), creating a favorable environment for air parcels to rise once triggered.

Crucially, the sharp decline in CAPE observed after 12:00 UTC, Figure 6(a) marks the phase of convective overturning. This indicates that the stored atmospheric potential energy was effectively consumed to drive the intense updrafts of the mature storm system, temporally correlating with the peak rainfall event. Complementing this energy analysis, Figure 6(c) and Figure 6(d) confirm deep tropospheric saturation and instability, with K-Index (KI) values exceeding 37 and Total Totals Index (TTI) surpassing 44.5 throughout the event.

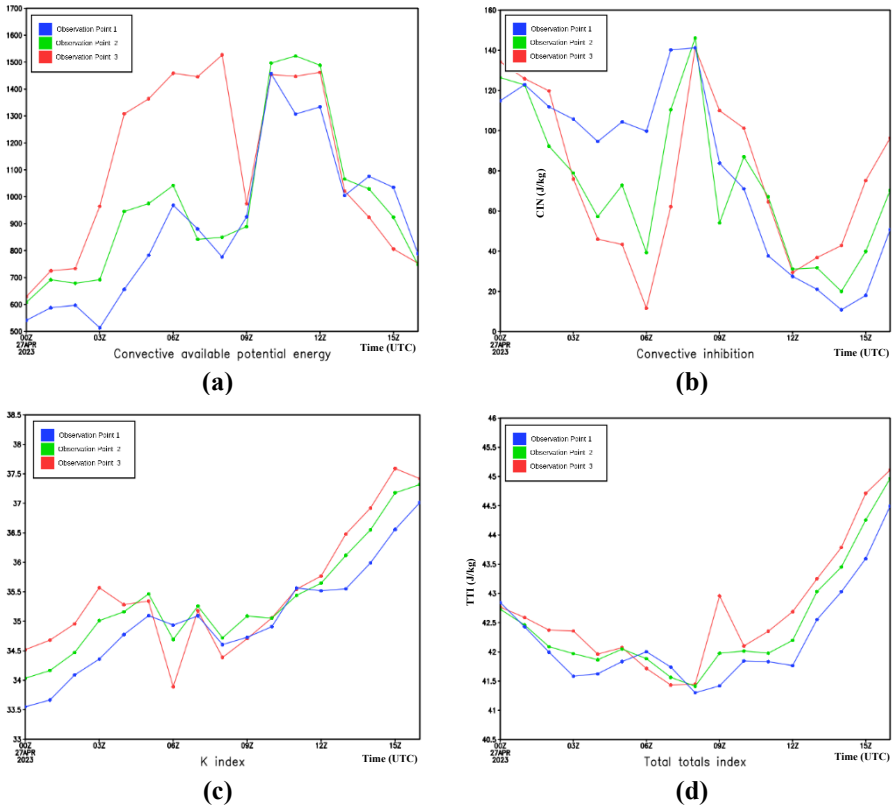

Figure 6 Atmospheric Instability Indices Charts: (a) CAPE, (b) CIN, (c) K-Index, and (d) TTI on April 27, 2023.

The detailed vertical atmospheric profile is observed through the Skew-T Log-P diagram in Figure 7. Observations at 00:00 UTC show a large positive area; however, by the 12:00 UTC observation, this area had significantly shrunk, and the CAPE value dropped sharply to 126.69 J/kg. This confirms the occurrence of the storm consumption phenomenon, where the potential energy accumulated during the day was fully released and consumed by the thunderstorms to produce the extreme rainfall that persisted throughout the night.

3.4 Coastal Convergence and Lifting Mechanisms

As the primary triggering mechanism for the aforementioned instability, the surface wind patterns at the 925 hPa level were analyzed in Figure 8. A significant convergence zone, a meeting of air masses, was identified along the Cilacap coastline. Sea breezes from the Indian Ocean, carrying high moisture, met with local land breezes, creating a vertical lifting force that pushed the air mass upward

to condense into clouds. The continuous moisture supply, further enhanced by MJO phase 4-5 activity, made this region highly productive in generating extreme rainfall.

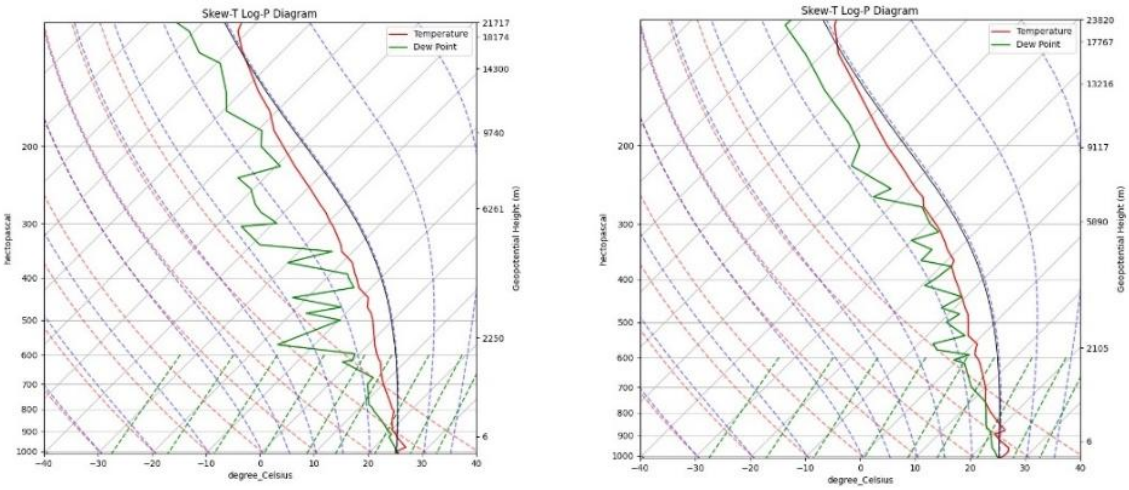

Figure 7 Profile of the sounding measurement results on the SkewT-logP diagram on April 27, 2023, for 00 UTC and 12 UTC.

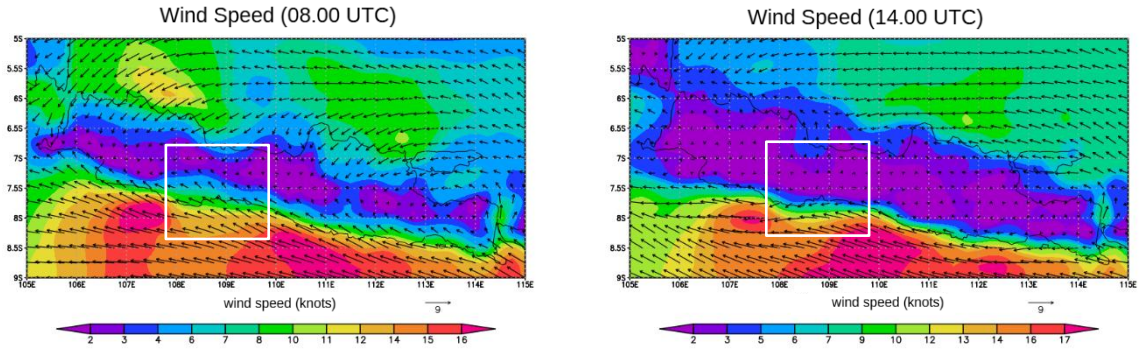

Figure 8 Wind Speed Distribution

4. CONCLUSION

Based on the diagnosis of atmospheric dynamics regarding the extreme flood event in Cilacap on April 27, 2023, it can be concluded that the disaster was triggered by the development of a highly intense mesoscale convective system. Atmospheric conditions prior to the event exhibited extreme instability, identified through quantitative thermodynamic parameters exceeding critical thresholds, specifically CAPE values above 1500 J/kg peaking between 09:00 and 12:00 UTC, CIN below 80 J/kg, and a K-Index exceeding 37. The development of Cumulonimbus (Cb) clouds was detected starting at 08:00 UTC, reaching full maturity at 15:00 UTC with cloud top temperatures (CTT) dropping to -70°C, which temporally aligned with the peak extreme rainfall intensity.

This extreme precipitation was mechanically driven by vertical lifting resulting from coastal convergence at the low-level (925 hPa), where the interaction between moisture-rich Indian Ocean sea breezes and local land breezes created a continuous energy supply. The energy conversion process during the storm was clearly recorded in the Skew-T diagram through the storm consumption phenomenon, marked by a sharp decline in CAPE observed at 12:00 UTC. This proves a massive release of atmospheric potential energy converted into kinetic energy, resulting in persistent heavy rainfall throughout the coastal region of Cilacap.

REFERENCE

Abay, F. M. J. (2021). Analisis Dinamika Atmosfer Dan Distribusi Awan Konvektif Menggunakan Teknik Red Green Blue (RGB) Pada Citra Satelit Himawari-8: Studi Kasus Banjir Jakarta 30 Desember 2019 - 1 Januari 2020. *Megasains*, *12*(1), 34–39.

Adiningsih, E. S., Sofan, P., & Prasasti, I. (2016). Pemanfaatan Teknologi Penginderaan Jauh untuk Monitoring Kejadian Iklim Ekstrem di Indonesia. *Jurnal Sumberdaya Lahan*, *10*(2).

Ahrens, C. D. (2015). *Meteorology today: an introduction to weather, climate, and the environment*. Cengage Learning Canada Inc.

Alfiansyah, A. , & N. F. (2020). Proses Konveksi dan Dampaknya Terhadap Curah Hujan di Wilayah Tropis. *Jurnal Meteorologi Dan Geofisika*, *14*(2), 45–56.

Alfred Sagala, E., Bangun, E., Subiyanto, A., & Sri Asmita, A. (2023). Pemanfaatan SATAID untuk Analisis Kondisi Atmosfer saat Banjir di Kalukku Menggunakan Metode Numerical Weather Prediction. *Jurnal Kewarganegaraan*, *7*(2).

Allen, M. R., & Ingram, W. J. (2002). Constraints on future changes in climate and the hydrologic cycle. *Nature*, *419*(6903), 224–232.

Arafat, K. N., Donny Harisuseno, & Jadfan Sidqi Fidari. (2024). Kajian Stabilitas Atmosfer Menggunakan Terhadap Kejadian Hujan yang Mempengaruhi Bencana Banjir Bandang. *Jurnal Teknologi Dan Rekayasa Sumber Daya Air*, *4*(02), 1578–1591.

Ayasha, N. (2021). A comparison of rainfall estimation using himawari-8 satellite data in different Indonesian topographies. *International Journal of Remote Sensing and Earth Sciences (IJReSES)*, *17*(2), 189–200.

Blanchard, D. O. (1998). Assessing the vertical distribution of convective available potential energy. *Weather and Forecasting*, *13*(3), 870–877.

Coiffier, Jean. (2011). *Fundamentals of numerical weather prediction*. Cambridge University Press.

Diniyati, E., Syofyan, D. Q., & Mulya, A. (2021). Pemanfaatan Satelit Himawari-8 dengan Metode NWP dan RGB untuk Menganalisis Kondisi Atmosfer Saat Banjir di Sidoarjo Tanggal 28 Mei 2020. *JPIG (Jurnal Pendidikan Dan Ilmu Geografi)*, *6*(1), 1–14.

Ferdiansyah, A. (2012). *Potensi parameter keluaran raob (rawinsonde observation programs) sebagai indikator kunci dalam analisis curah hujan*.

Hadiansyah, R., Indranata, A. L., Silitonga, A. K., & Winarso, P. A. (2019). Kajian Kondisi Atmosfer Saat Kejadian Hujan Ekstrem di Padang Sumatera Barat (Studi Kasus Tanggal 14 Februari 2018). *Prosiding SNFA (Seminar Nasional Fisika Dan Aplikasinya)*, *3*, 246–257.

Iman Yuda Saputra. (2023, April 28). Kota Cilacap Diterjang Banjir, BMKG Ungkap Penyebabnya. *SOLOPOSJATENG*.

Istrate, V., Dobri, R. V., Bărcăcianu, F., Ciobanu, R. A., & Apostol, L. (2021). Sounding-derived parameters associated with severe hail events in Romania. *Időjárás*, *125*(1), 39–52.

Kachi, M. (2012). Overview of Global Satellite Mapping of Precipitation (GSMaP). *The 6th World Water Forum, March*.

L, A. I. R. W. S. S. A. F. B. I. (1990). *The Use of the Skew T, Log P Diagram in Analysis and Forecasting. Revision*.

Lillesand, T., Kiefer, R. W., & Chipman, J. (2015a). *Remote sensing and image interpretation*. John Wiley & Sons.

Lillesand, T., Kiefer, R. W., & Chipman, J. (2015b). *Remote sensing and image interpretation*. John Wiley & Sons.

Lv, X., Guo, H., Tian, Y., Meng, X., Bao, A., & De Maeyer, P. (2024). Evaluation of GSMaP Version 8 Precipitation Products on an Hourly Timescale over Mainland China. *Remote Sensing*, *16*(1), 210.

Muttaqin, A., M. F. N., & A. P. A. (2016). Analisis Profil CAPE (Convective Available Potential Energy) Selama Kegiatan Intensive Observation Periode di Dramaga Bogor. *Jurnal Sains & Teknologi Modifikasi Cuaca*, *17*(2), 83–89.

Nurlatifah, A., Hatmaja, R. B., & Rakhman, A. A. (2023). Analisis Potensi Kejadian Curah Hujan Ekstrem di Masa Mendatang Sebagai Dampak dari Perubahan Iklim di Pulau Jawa Berbasis Model Iklim Regional CCAM. *Jurnal Ilmu Lingkungan*, *21*(4), 980–986.

Pu, Z., & Kalnay, E. (2018). Numerical Weather Prediction Basics: Models, Numerical Methods, and Data Assimilation. In *Handbook of Hydrometeorological Ensemble Forecasting* (pp. 1–31). Springer Berlin Heidelberg.

Rachman, A. F., H. H., & D. S. (2020). Pemanfaatan Citra Satelit Himawari-8 untuk Pemantauan Cuaca di Wilayah Asia-Pasifik. *Jurnal Meteorologi Dan Geofisika*, *14*(1), 23–32.

Rozi, M. F. (2019). Prediksi pertumbuhan awan cumulonimbus pada citra himawari ir enhanced menggunakan deep echo state network (deepesn). *Universitas Islam Negeri Sunan Ampel Surabaya*.

Rusdin, A. A., Palloan, P., Subaer, S., & Prasetiyo, A. (2023). Uji Akurasi Ambang Batas Indeks Stabilitas Atmosfer Terhadap Pembentukan Thunderstorm dan Awan Cumulonimbus di Stasiun Meteorologi Kelas I Sultan Hasanuddin. *Jurnal Fisika Unand*, *12*(2), 268–274.

Saputra, A. I., & Yahya Darmawan. (2025). Analisis Hujan Ekstrem Menggunakan Data Satelit Himawari 9, Model, dan Observasi (Studi Kasus: Jakarta Utara, 29 Februari 2024). *Jurnal Penelitian Fisika Dan Terapannya (JUPITER)*, *6*(2), 9–21.

Sari, D. P., & S. A. (2021). Analisis Citra Natural Colour dan IR Enhanced dari Satelit Himawari-8 dalam Pengamatan Cuaca Ekstrem. *Jurnal Penelitian Atmosfer Dan Meteorologi*, *9*(3), 45–58.

Setiawan, A., W. D., & A. R. (2019). Analisis Stabilitas Atmosfer dengan Menggunakan K-Index untuk Memprediksi Hujan Lebat di Wilayah Indonesia. *Jurnal Meteorologi Dan Geofisika*, *17*(2), 45–52.

Setiawan, A., Hutagalung, M., Adhitiansyah, D., Humairah, N., & Mulya, A. (2021). Kajian Kondisi Atmosfer Saat Kejadian Hujan Lebat Penyebab Banjir Di Kota Palembang (Studi Kasus Tanggal 13 September 2021). In *Jurnal Material dan Energi Indonesia* (Vol. 11, Issue 02).

Shuman, F. G. (1989). History of numerical weather prediction at the National Meteorological Center. *Weather and Forecasting*, *4*(3), 286–296.

Siti Aisah, N., & S. B. M. (2021). Pengaruh Variabilitas Stratosfer Terhadap Pola Cuaca Ekstrem di Indonesia. *Jurnal Atmosfer Indonesia*, *8*(1), 67–78.

Stull, R. B. (2012). *An introduction to boundary layer meteorology* (Vol. 13). Springer Science & Business Media.

Stull, R. B. (2015). *Practical meteorology: an algebra-based survey of atmospheric science*. University of British Columbia.

Syahputra, R., Darmawan, Y., Tinggi Meteorologi Klimatologi dan Geofisika, S., Bintaro Utara Jl Perhubungan No, J. I., Betung, P., Pd Aren, K., & Tangerang Selatan, K. (n.d.). *Pemanfaatan Teknik Rgb Pada Citra Satelit Himawari-8 Untuk Analisis Dinamika Atmosfer Kejadian Banjir Kabupaten Bandung 06 Mei 2023 Utilization Of Rgb Techniques In Satellite Imagery Himawari-8 For Atmospheric Dynamics Analysis Flooding Event In Bandung District 06 May 2023*. *15*(1), 37–43.

Trenberth, K. E., Fasullo, J. T., & Mackaro, J. (2011). Atmospheric moisture transports from ocean to land and global energy flows in reanalyses. *Journal of Climate*, *24*(18), 4907–4924.

Wallace, J. M., & Hobbs, P. V. (2006). *Atmospheric science: an introductory survey* (Vol. 92). Elsevier.